university of groningen

BACHELOR'S THESIS CHEMISTRY

Faculty of Science and Engineering

Determination of pancake aromaticity by means of ring current analysis on transition-metal-complexes

Kieran Engel S3429679
Under supervision of Dr. R.W.A Havenith
Second assessor Dr. J. E. M. N. Klein
Submitted on 21-11-2020

$[Ti(P_5)_2]^{2-}$ is a compound that was researched to conclude the oxidation state of the titanium-centre. In the analysis a ring current stretching in the direction of its pancake bonds was discovered and it raised the question whether pancake bonds could be deemed aromatic. Therefore, the ring currents of the molecules $[Ti(P_5)_2]^{2-}$ and its analogues $[Sc(P_5)_2]^{3-}$, $[V(P_5)_2]^{-}$, $[Cr(P_5)_2]$, $[Mn(P_5)_2]^{+}$, $[Zr(P_5)_2]^{2-}$ and ferrocene were analysed to give insight in the aromaticity of these compounds. All of the complexes, except $[Sc(P_5)_2]^{3-}$, retain their diatropic current and thus aromaticity in the ligand ring. The diatropic currents in the direction of the pancake bonds only have a significant density for $[Ti(P_5)_2]^{2-}$ and ferrocene. For $[V(P_5)_2]^{-}$ and $[Zr(P_5)_2]^{2-}$ there is still a hardly visible diatropic ring current. The vanishing of ring currents at $[Sc(P_5)_2]^{3-}$ and $[Cr(P_5)_2]$ could be due to an increase in ring-to-ring distance and a lowering of the energy of the 3d-orbitals, respectively. A direct correlation between the aromaticity and the pancake bonds is, however, still missing.

Introduction

Ever since the discovery of the structure of benzene by Kekulé, additional criteria for what constitutes an aromatic compound have come to light and have been researched. Through the years, the aromaticity of a compound has been identified by means of thermodynamic stability, delocalised carbon-carbon bond lengths, Hückels rule and magnetic ring current effects, and so forth[1,2]. The latter was discovered when benzene was analysed in the magnetic field of an ^{1}H-NMR spectrometer. They observed that the chemical shift of the hydrogens lies more downfield than what theoretically was predicted. As suggested, the hydrogens are affected by a stronger magnetic field than what is induced by the NMR-machine[3]. The benzene ring creates its own magnetic field as the delocalisation of the π-electrons causes them to move in a circular motion. This ring current of electrons produces its own magnetic field, and is opposite to the induced field in the centre of the molecule. However, it is augmenting the magnetic field on the outside of the ring[4]. Hence, the magnetic environment near the hydrogens is increased as is depicted in figure 1. This phenomenon can be linked to aromaticity through Hückels rule. Hückel stated in his theorem that systems with 4n+2 π-electrons are deemed aromatic and systems with 4n π-electrons are anti-aromatic. As it turns out, aromatic compounds display a diamagnetic current and anti-aromatic compounds have a paratropic current[5].

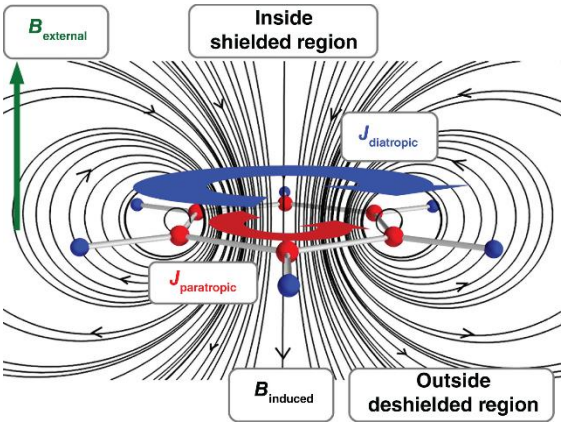

Fig. 1 *The induced magnetic field within benzene and the direction of a para- and diamagnetic current[4].*

In the aftermath of this discovery, it became a highly used method in assessing the aromaticity of a compound[4]. *Nunes dos Santos Comprido et al.*[6] aimed to appoint the oxidation state to a titanium atom in a complex analogous to ferrocene, $[Ti(P_5)_2]^2$. This compound had been previously made by *Urnėžius et al.*[7]. However, assigning a formal oxidation state to the titanium centre proved more arduous than expected. The phosphorus-rings were established to be non-innocent ligands, i.e. ligands in a metal-complex that obscure the oxidation state of the metal. *Nunes dos Santos Comprido et al.*[6] stated that a more reduced

titanium would show ring currents in the P_5-rings similar to ferrocene and a paratropic ring current would be present if the titanium is oxidised due to the ligand rings having a system of 8π-electrons. However, unexpectedly an additional ring current was observed perpendicular to the P_5-rings. This led to an implication of a so-called ring current due to pancake bonds[6].

Pancake bonding is a form of π-π interaction between two aromatic rings[8]. The delocalised π-system, present in aromatic rings, creates a quadrupole moment. One that manifests itself in a partial negative charge (δ^-) above and below the ring and a partial positive charge (δ^+) in the plane of the molecule. In terms of π-stacking, the face-centred conformation is the energetically least favourable as opposed to the favourable off-centre parallel and t-shaped stacking shown in figure 2[9]. Face-centred stacking is the conformation in pancake structures, however the pancake bonds make it a feasible conformation which counteract the quadrupole-quadrupole repulsion. They are formed between radicals or multiradicaloid ground states[8]. The singly occupied molecular orbitals (SOMO) of the radicals will overlap with each other and create a doubly occupied highest occupied molecular orbital (HOMO) which lies lower in energy and thus stabilizes the molecule[10].

Since the titanium-complex has a ring current stretching the pancake bond and ferrocene does not[11], it was thought that the aromaticity from ring to ring would be lost going from titanium to iron. This research aims to validate the existence of aromaticity in these pancake structures, particularly for this series of metal-complexes similar to $[Ti(P_5)_2]^{2-}$. The metal-centre is interchanged along the periodic table ranging from scandium to manganese with the extension of zirconium. The charge on each system is thereby altered to give isoelectronic compounds. Additionally, ferrocene will be examined in the same manner. The induced magnetic field shall be going in the direction of z as well as x or y, as indicated in the coordinate system of figure 3. This is expected to induce a ring current for the phosphorus-ring and for the whole molecule, respectively. The electrons in the π-orbitals are in a delocalised system and are, therefore, able to circulate which gives rise to a ring current. Thus, in this research a spectral analysis of the π-orbitals will be examined only, as they bear the greatest contribution to the ring current[12]. As mentioned before, the aromaticity can be inferred from the direction of the ring current. It is expected that the diatropic current of the pancake bond will disappear somewhere going from $[Ti(P_5)_2]^{2-}$ to $[V(P_5)_2]^-$, $[Cr(P_5)_2]$, $[Mn(P_5)_2]^+$ and ferrocene. This could be a consequence of the increasing d-character of the pancake molecular orbitals (MOs) as they will shift downwards, i.e. towards the d-orbitals of the metal, as the metal increases its atomic number. When these MOs start to take on more d-character, the pancake bond could be lost and thus the ring current it causes. Thereby, assuming that the pancake bond indeed causes the ring current in the titanium-complex.

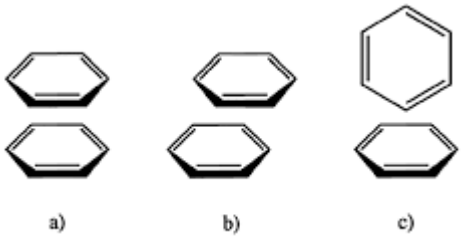

Fig. 2 *π-π stacking of benzene as (a) face-centred, (b) off-centre, (c) t-shaped*[9].

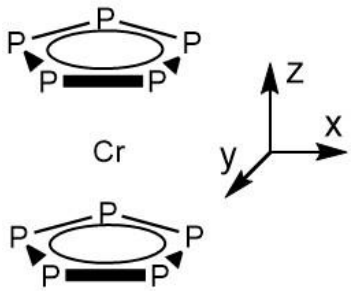

Fig. 3 *The position of the metal-complexes in the coordinate system.*

Theory

In defining a Schrödinger equation for a quantum system with a magnetic field, a perturbation is applied to the reference Hamiltonian. $\hat{H}_0$ is the reference Hamiltonian and $\hat{H}_1$ is the first-order perturbation in equations (1) and (2). Furthermore, the angular momentum operator and the magnetic field are represented by $\hat{L}$ and B, respectively[13].

$$\hat{H}_0 = -\frac{\hbar^2}{2m_e}\sum_{i=1}^{n}\nabla_i^2 + V \quad (1)$$

$$\hat{H}_1 = \frac{e}{2m_e}\hat{L} \times B \quad (2)$$

$$\hat{H} = \hat{H}_0 + \lambda\hat{H}_1 \quad (3)$$

λ is an added parameter which signifies the strength of the perturbation with a value between 0 and 1. However, for derivation purposes it does not matter what value λ takes on. With an added perturbation of the first-order, the Schrödinger equation (4) with E and Ψ being expanded in series (5) and (6), respectively, gives equation (7)[14].

$$\hat{H}\Psi = E\Psi \quad (4)$$

$$E = E_0 + \lambda E_1 + \lambda^2 E_2 + \ldots \quad (5)$$

$$\Psi = \Psi_0 + \lambda\Psi_1 + \lambda^2\Psi_2 + \ldots \quad (6)$$

$$\left(\hat{H}_0 + \lambda\hat{H}_1\right)(\Psi_0 + \lambda\Psi_1 + \lambda^2\Psi_2 + \cdots) = (E_0 + \lambda E_1 + \lambda^2 E_2 + \ldots)(\Psi_0 + \lambda\Psi_1 + \lambda^2\Psi_2 + \ldots) \quad (7)$$

Factoring out the λ, results in equations for each order of perturbation. Equation (8), which states that the first-order energy is equal to the expectation value of the first-order perturbation acting on the ground-state wavefunction, can be derived from the first-order equation.

$$E_1 = <\Psi_0\left|\hat{H}_1\right|\Psi_0> \quad (8)$$

Known from the solvable zeroth-order Schrödinger equation is that all the eigenfunctions of $\hat{H}_0$ form an orthogonal basis set. The reference wavefunction, Ψ_0, obtained from this equation is chosen as the lowest and is therefore the ground state of this quantum system. This indicates that the other eigenfunctions of the set belong to all possible excited states. Taking the sum over all these states will result in the first-order wavefunction which can be seen in equation (9)[13,14].

$$\Psi_1 = -\frac{e}{2m_e}\sum_{j>i}\Psi_j\frac{<\Psi_j|\hat{L}\times B|\Psi_i>}{E_j - E_i} \quad (9)$$

Having a perturbation applied to the system brings about a complication when it comes to the origin of the system and the outcome of the current density $j(r)$ to the first-order (10).

$$j(r) = \frac{e}{2m_e}B \times (r-d)\rho_0(r) + \frac{ie\hbar N}{m_e}\int[\Psi_0\nabla\Psi_1 - \Psi_1\nabla\Psi_0]d\tau' = j^{(d)}(r) + j^{(p)}(r) \quad (10)$$

d is the chosen origin of the coordinate system in addition to the point of rotation for the angular momentum operator. The first term of this equation is the expectation value of the first-order energy as described in equation (8) and the second term is the applied perturbation. The expectation value and the perturbation have a different degree of accuracy and both terms are dependent on d. Therefore, altering the origin will result in deviant current densities[13]. *Keith et al.*[15] created an approach to overcome this obstacle called continuous transformation of origin of current density-diamagnetic zero (CTOCD-DZ). The origin is chosen to be equal to the point where the current density is calculated, i.e. d equal to r, every time (ipsocentric) which causes the first term of equation (10) to become zero and thus eliminates the dependency on d.

$j^{(d)}(r)$ and $j^{(p)}(r)$ from equation (10) are the diamagnetic and paramagnetic contributions to the ring current, respectively. The direction of the current and why it arises is an electromagnetic concept. Faraday states that a change in magnetic flux, normal to an electrical circuit, will induce a current. The change in

	E	$2C_5$	$2(C_5)^2$	$5C'_2$	σ_h	$2S_5$	$2(S_5)^3$	$5\sigma_v$	linear, rotations	quadratic
A'_1	1	1	1	1	1	1	1	1		x^2+y^2, z^2
A'_2	1	1	1	-1	1	1	1	-1	R_z	
E'_1	2	$2\cos(2\pi/5)$	$2\cos(4\pi/5)$	0	2	$2\cos(2\pi/5)$	$2\cos(4\pi/5)$	0	(x, y)	
E'_2	2	$2\cos(4\pi/5)$	$2\cos(2\pi/5)$	0	2	$2\cos(4\pi/5)$	$2\cos(2\pi/5)$	0		(x^2-y^2, xy)
A''_1	1	1	1	1	-1	-1	-1	-1		
A''_2	1	1	1	-1	-1	-1	-1	1	z	
E''_1	2	$2\cos(2\pi/5)$	$2\cos(4\pi/5)$	0	-2	$-2\cos(2\pi/5)$	$-2\cos(4\pi/5)$	0	(R_x, R_y)	(xz, yz)
E''_2	2	$2\cos(4\pi/5)$	$2\cos(2\pi/5)$	0	-2	$-2\cos(4\pi/5)$	$-2\cos(2\pi/5)$	0		

Fig. 4 *Character table of point group* D_{5h}.

magnetic flux can be realised by a number of actions, e.g. magnetic field strength change over time or a change in the circuits position over time. However, for quantum mechanical systems a change in flux is not required. The direction of the electric current in the circuit is determined by the right-hand-rule, as Lenz's law declares that the current will always be in such a direction that the generated magnetic field opposes the induced magnetic field[16]. Thus, according to classical concepts the current will only have diamagnetic contributions. However, a paratropic current is completely due to quantum mechanical effects in the form of a sum-over-states[13].

With the CTOCD-DZ approach the first term of (10) becomes zero and is reduced to the sum-over-states. This sum-over-states is now responsible for the diatropic and paratropic contributions to the total current density. Equation (9) can be split in to two terms, one of which is dependent on the linear momentum operator $\hat{P}$. The other term is dependent on the angular momentum operator which is now written as $\hat{L}(0)$, since it rotates about the origin. This gives the following equation (11).

$$\Psi_1 = \frac{e}{2m_e}\left[\sum_{j>i}\Psi_j \frac{<\Psi_j|\hat{L}(0)|\Psi_i}{E_j-E_i}\right]\cdot B + \frac{e}{2m_e}\left[d\times\sum_{j>i}\Psi_j \frac{<\Psi_j|\hat{P}|\Psi_i}{E_j-E_i}\right]\cdot B = \Psi_1^{(p)} + \Psi_1^{(d)} \quad (11)$$

Depending on the nature of an excitation, i.e. due to $\hat{P}$ or $\hat{L}(0)$, the contribution to either a diatropic or a paratropic current can be inferred. $\hat{P}$ and $\hat{L}(0)$ give rise to translational and rotational transitions, respectively. *Steiner et al.*[5] established therein selection rules which dictate the contribution of each orbital based on their symmetry. If the product of a transition from an occupied to unoccupied orbital results in a symmetry containing x, y or z, then the contribution to the current will be diamagnetic. On the other hand, may the symmetry product contain a symmetrical group that goes with Rx, Ry or Rz then the current is paramagnetic of nature. Note, however, that it depends on the direction of the magnetic field as well. If the magnetic field is in the z-direction then a translational transition of x/y and a rotational transition of Rz will be necessary to bring forth a diamagnetic or paramagnetic current, respectively[5]. In this research only complexes of the D_{5h} point group are examined. Thus, the character table for D_{5h}, figure 4, determines the possible symmetries for transitions, i.e. E_1' or A_2'' for translations and E_1'' or A_2' for rotations.

Experimental

Ferrocene was made with D_{5h} conformation and the geometry was optimised using the basis set cc-pVDZ and DFT B3LYP using the program GAMESS-UK[17,18]. The ring

Table 1 *Directions of the magnetic field in each plotting plane*

Plotting plane	Direction magnetic field
All complexes (A)	0.1z
Ferrocene (B)	-0.1 x
Ferrocene (C)	0.9507x – 0.3102y
$[Ti(P_5)_2]^{2-}$ (B)	0.8083x – 0.5888y
$[Ti(P_5)_2]^{2-}$ (C)	-0.1y
$[V(P_5)_2]^{-}$ (B)	-0.1x
$[V(P_5)_2]^{-}$ (C)	-0.7363x +0.6766y
$[Cr(P_5)_2]$ (B)	0.1y
$[Cr(P_5)_2]$ (C)	0.8083x + 0.5888y
$[Sc(P_5)_2]^{3-}$ (B)	0.1y
$[Sc(P_5)_2]^{3-}$ (C)	-0.8083x + 0.5888y
$[Zr(P_5)_2]^{2-}$ (B)	0.1y
$[Zr(P_5)_2]^{2-}$ (C)	0.8083x + 0.5888y

currents were calculated with GAMESS-UK and SYSMO[19] (mo800) for which the ligand of the optimised molecule was placed in the xy-plane, which is parallel to plane A in figure 5. Three different plotting planes were used to observe the overall ring current. The first plane (A) is 1 bohr above and parallel to one of the P_5-rings, the second plane (B) is through two adjacent phosphors in the phosphorus-ring and in the z-direction. The last plane (C) is in the z-direction as well, however going through one phosphor and the centre of the molecule, i.e. the corresponding transition metal. In the first plane one can observe the ring current that is induced in an individual P_5-ring. The pancake ring current, provided there is one, is visible in the two latter defined planes. The magnetic field is perpendicular to each respective plotting plane. Additionally, the magnetic field is out of the plane of the paper in the ring current figures, meaning diamagnetic currents are portrayed as anti-clockwise and paramagnetic currents are clockwise. With the magnetic field being perpendicular to the plotting planes, the field's direction changes with it, see table 1. In terms of gauge origin choice, the CTOCD-DZ approach is utilised.

Afterwards, the complexes $[Sc(P_5)_2]^{3-}$, $[Ti(P_5)_2]^{2-}$, $[V(P_5)_2]^{-}$, $[Cr(P_5)_2]$, $[Mn(P_5)_2]^{+}$ and $[Zr(P_5)_2]^{2-}$ were made in the D_{5h} conformation followed by a geometry

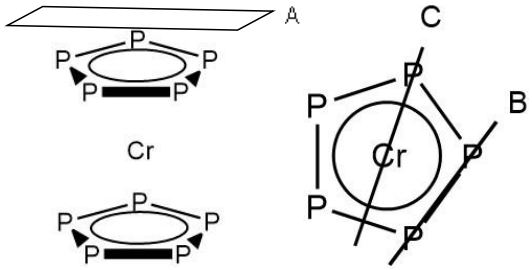

Fig. 5 *The plotting planes A, B and C used to render and visualise the ring currents.*

Table 2 *π-orbitals of each complex that were used for ring current analysis*

Complex	π -orbitals
$[Fe(Cp)_2]$	32, 41, 42, 43, 44, 45
$[Sc(P_5)_2]^{3-}$	71, 77, 80, 81, 84, 85, 86, 87
$[Ti(P_5)_2]^{2-}$	71, 79, 80, 81, 84, 85, 86, 87
$[V(P_5)_2]^{-}$	71, 79, 80, 81, 84, 85, 86, 87
$[Cr(P_5)_2]$	71, 79, 80, 81, 84, 85, 86, 87
$[Zr(P_5)_2]^{2-}$	66, 72, 75, 76, 79, 80, 81, 82

optimisation. The cc-pVDZ basis set was used in combination with the B3LYP functional. Except for zirconium, for which the cc-pVDZ-PP basis set was used. Accordingly, the charge on each complex was altered to generate isoelectronic molecules. Subsequently, hessian calculations were performed to check the nature of the stationary states. The ring currents were calculated in the same plotting planes and program as mentioned before. Two sets of orbitals were used in the ring currents for each system, i.e. there is a visualisation of the total combined orbitals and a visualisation of solely the π-orbitals, see table 2 for the used π-orbitals.

To get the symmetry of the ligands, i.e. $(P_5)_2^{6-}$, for the MO-diagram, SCF calculations were performed using Gaussian16[20] (B3LYP, cc-pVDZ). The distance between the rings and the length of the P-P bonds were taken from the optimised $[Ti(P_5)_2]^{2-}$ geometry. Additionally, the same was done to get the symmetries of the titanium-complex MOs. A Mulliken population analysis was performed on the SCF (B3LYP, cc-pVDZ) orbitals for the titanium- and chromium-complexes. Ultimately, the contributions of excitations regarding the scandium-, titanium-, chromium-complex and ferrocene were calculated with mo801. The program generates values which represent the contribution of each excitation to a ring current. These values are in fact the coefficients in the first-order wavefunction equation (9) or $\frac{<\Psi_j|\hat{O}|\Psi_i>}{E_j - E_i}$, in which $\hat{O}$ can be the angular or linear momentum operator.

Appendix A describes how all calculations and results are organised and stored within the files of the peregrine cluster.

Results and discussion

$[Fe(C_5H_5)_2]$

According to the donor-pair method for metal-complexes, the cyclopentadienyl ligand (Cp) is negatively charged and contributes six electrons per ring to the complex. The iron, on the other hand, becomes positively charged with a formal oxidation state of two, i.e. Fe(II). In total this makes it an 18-electron compound. *Bean et al.*[11] presented their D_{5h} ferrocene MO-diagram, however figure 6 is an alteration of that diagram with the order of MOs defined by GAMESS-UK (B3LYP). The MOs are assigned an irreducible representation according to the D_{5h} point group.

As can be seen in appendix B1, the cyclopentadienyl ligand has a strong

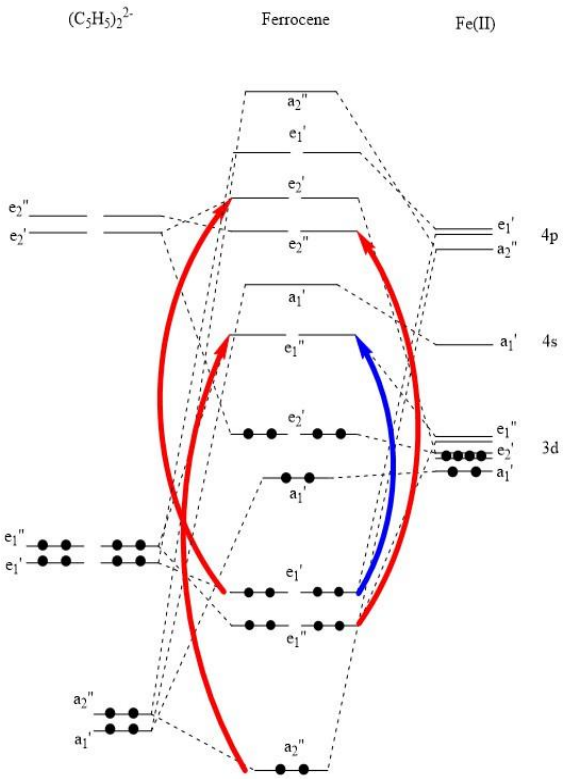

Fig. 6 *MO-diagram of ferrocene (D_{5h}) with x/y-(red) and z-translations (blue).*

diatropic current. To obtain a diamagnetic current here, an irreducible representation conform with a translation in the x- or y-direction is needed, i.e. E_1'. Considering the product table of D_{5h} and transitions from occupied π-orbitals to unoccupied orbitals, the following transitions are of importance for the Cp and overall ring current: $E_1'' \rightarrow E_2''$, $E_1' \rightarrow E_2'$ and $A_2'' \rightarrow E_1''$, which are depicted in figure 6. The diamagnetic ring current of the Cp is in accordance with *Steiner et al.*[5] theory that an aromatic ring with 4n+2 π-electrons will acquire a diamagnetic ring current, the ring has six π-electrons.

Where the π-system of plane B portrays a nearly interrupted current in the middle and the top and bottom seem to have a higher current density. The total system does have a more distinct ring current and a lot of activity in the middle of the ligands. The magnetic field in plane B is in the x-direction, meaning that the diatropic current is caused by either a y- or z-translation. The z-transition is of symmetry A_2" and is

depicted by the blue arrow in figure 6 with a contribution of 1.703. An additional z-translation falls out of the MO-diagram going from orbital 41 (A_2") to 63 (A_1') and has a contribution of 1.242. The magnetic field of ferrocene in plane C is a linear combination of directions x and y, as described in table 1 in the experimental. This does not matter for the transitions, considering x and y are degenerate and share the same symmetry transitions. The ring current appears in a diamagnetic direction albeit disorganised. This can be caused by either x-, y- or z-transitions, however this current is debatably a ring current.

$[Ti(P_5)_2]^{2-}$

As has been discussed before, it becomes debatable what the formal oxidation is of the metal centre in the titanium-complex. However, the oxidation chosen for this research is IV with the help of *Nunes dos Santos Comprido et al.*[6]. This means that a total of 16 π-electrons is attributed to the two ligands, as each ring has its own six π-electrons and on top of that the four valence-electrons of titanium.

Appendix B2 shows all ring currents of $[Ti(P_5)_2]^{2-}$. Noticeably, the π-orbitals contribute not as much to the ring current limited to the P_5-ring as in ferrocene. This current could be due to x- and y-translations $E_1'' \rightarrow E_2''$ in figure 7 (above) with a value of 1.08. Naturally, this transition is also present in the MO-diagram of the rings alone. Another $E_1'' \rightarrow E_2''$ translation with a comparable value is present, however not displayed in the diagram as it goes to much higher lying MOs, namely MOs 100 and 101. Figure 8 exhibits the numbers of the MOs that are visible in the MO-diagrams discussed here. The molecule's B and C planes exhibit a neat diatropic ring current around the whole molecule. The transition for this current can be x-, y- or z-oriented. One major contribution to this diatropic current is from the four degenerate HOMO-electrons that have a virtual transition from

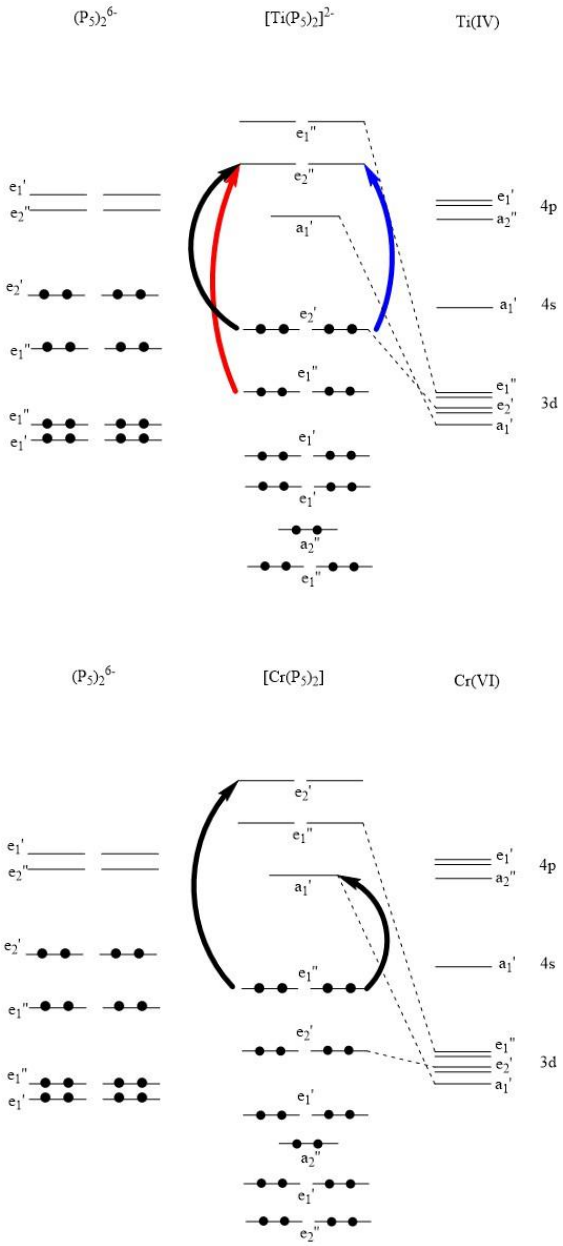

***Fig. 7** MO-diagrams of $[Ti(P_5)_2]^{2-}$ (above) and $[Cr(P_5)_2]$ (below) with x/y- (red), z- (blue) and Rx/y-transitions (black).*

$E_2' \rightarrow E_2''$ (z-translation), which has a value of 2.755 according to mo801. For convenience, the MO-diagrams are portrayed like this even though the atomic orbitals (AOs) of the metal are in fact much lower in energy than the MOs of the ligands.

Furthermore, a novel phenomenon occurs where the metal centre shows a ring current of its own in a paramagnetic direction. The induced magnetic field, being in the y-direction, signifies a paratropic contribution due to an Ry-transition. Ry is of the

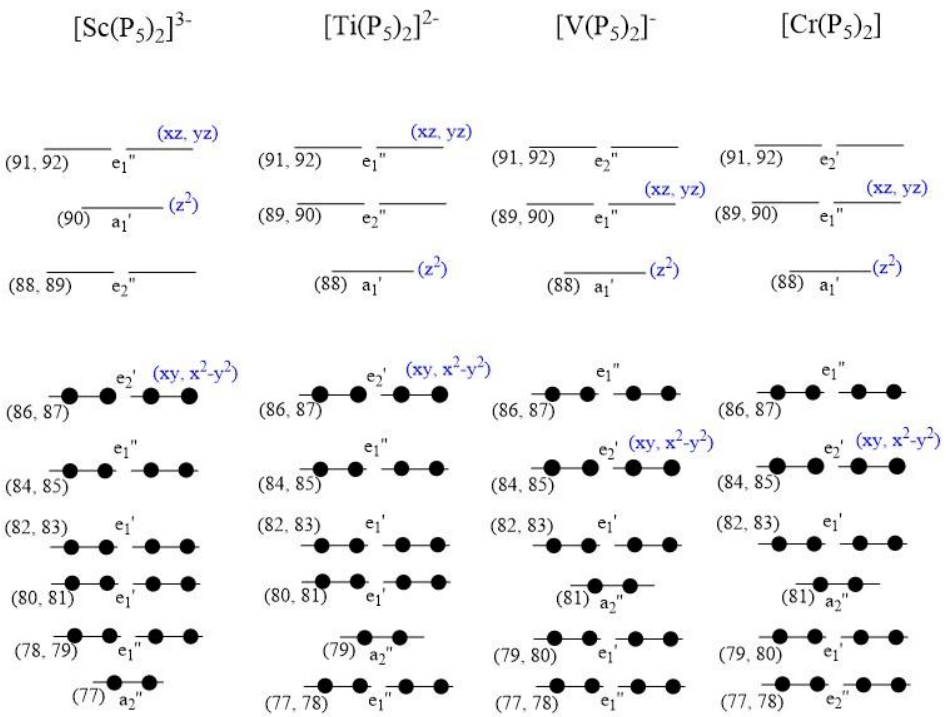

Fig. 8 *MO-diagrams of $[Sc(P_5)_2]^{3-}$, $[Ti(P_5)_2]^{2-}$, $[V(P_5)_2]^{-}$ and $[Cr(P_5)_2]$ with the respective MO-numbers and the 3d-orbitals.*

Table 3 *group populations of electrons on the d-orbitals of $[Ti(P_5)_2]^{2-}$ and $[Cr(P_5)_2]$*

Orbitals	$[Ti(P_5)_2]^{2-}$	$[Cr(P_5)_2]$
Ti-86/Cr-84	0.393	0.623
Ti-87/Cr-85	0.393	0.623
Ti-88/Cr-88	0.797	0.744
Ti-91/Cr-89	0.325	0.385
Ti-92/Cr-90	0.326	0.385

symmetry E_1'' and it can be realised through the black transition with a high contribution of 9.689 on average. The other major contributors go from E_1'' to MOs 93, 94 (E_2') and 97 outside of the diagram.

What can be established from the shape of the orbitals in appendix C, is that the E_2' HOMO is of dxy and dx^2-dy^2 character, in correspondence with the 3d-orbitals of the metal-centre. The A_1' and the E_1'' lowest unoccupied molecular orbitals (LUMOs) are dz^2 and dxz, dyz in character, respectively. The d-character, or electron population, of these orbitals can be found in table 3. Furthermore, the shape of MOs Ti-80 and Ti-81, shown in appendix C, give good representations of the pancake bonds that stretch from ring to ring. The remaining MOs of importance are displayed in appendix C.

$[Cr(P_5)_2]$

The first derivative of the energy to the coordinates exceeds the set threshold of 0.0005 by roughly 0.0006. Thus, the geometry of the complex has not reached true optimisation. However, the results of the hessian calculation are adequate and a further optimisation would not change the outcome of the ring currents and orbitals considerably.

When the transition metal changes from titanium to vanadium to chromium, i.e. to the right in the periodic table, the diatropic ring currents in plane B and C seem to decrease in intensity as seen in the figures in appendices B3 and B4. To the contrary, the paratropic current at the transition metal increases in size. The metal could be drawing in the electrons more into the centre, because of the higher positive charges on the metal.

The MO-diagram of the chromium-molecule is shown in figure 7 (below)

Table 4 *contribution values to the ring current of individual virtual excitations*

Transition type	Symmetry	Complex	MOs	Contribution value
x/y	$E_1'' \rightarrow E_2''$	$[Ti(P_5)_2]^{2-}$	84/85 → 89/90	1.08
		$[Cr(P_5)_2]$	86/87 → 93/94	0.92
		$[Sc(P_5)_2]^{3-}$	84/85 → 88/89	1.14
		$[Ti(P_5)_2]^{2-}$	84/85 → 100/101	1.21
		$[Cr(P_5)_2]$	86/87 → 101/102	1.25
		$[Sc(P_5)_2]^{3-}$	84/85 → 98/99	1.20
z	$E_2' \rightarrow E_2''$	$[Ti(P_5)_2]^{2-}$	86/87 → 89/90	2.75
		$[Cr(P_5)_2]$	84/85 → 93/94	1.90
		$[Sc(P_5)_2]^{3-}$	86/87 → 88/89	3.34
Rx/y	$E_1'' \rightarrow E_2'$	$[Ti(P_5)_2]^{2-}$	84/85 → 93/94	6.44
		$[Cr(P_5)_2]$	86/87 → 91/92	10.54

together with two Rx/y-transitions. The rotation, $E_1'' \rightarrow A_1'$, is prominent by being a transition from HOMO to LUMO and therefore it has a contribution of 22.30. The other transition $E_1'' \rightarrow E_2'$ is the same one described in the titanium-complex, now with an elevated contribution of 10.54. The other x-, y- and z-translations similar to $[Ti(P_5)_2]^{2-}$ outside of the diagram have decreased in value, table 4. It can be seen in plane A that the ring current is the same as with the titanium-complex.

Viewing the MO-diagrams of these complexes, a shift of MOs is noticeable which could explain these changes, see figure 8. The main differences in the relative positions of the MOs between $[Cr(P_5)_2]$ and $[Ti(P_5)_2]^{2-}$ involve the switching of E_2' and E_1'' at the HOMO and the rising of the E_2'' LUMO which draws in the E_1'' LUMO towards the HOMO. This could be interpreted as the MOs comprised of the 3d-orbitals shifting downwards. Inherently, the shape would have to resemble the d-orbitals more clearly which is complicated to make out of the pictures of the orbitals, because the MOs have the same shape as in the titanium-complex MOs. Therefore, a group population analysis is made of the 3d-orbitals of the titanium- and chromium-complexes. The d-character of orbitals Cr-84 and Cr-85, displayed in table 3, increase significantly. Furthermore, Cr-89 and Cr-90 have a slightly higher d-character and Cr-88 is actually lower in d-character than Ti-88. This is in accordance with the shifting of the MOs, because MO 88 is relatively situated in the same place and the others have shifted downwards in the chromium-complex MO-diagram. Thus, primarily the orbitals Cr-84 and Cr-85 gain d-character and are the cause for the z-transition. Table 4 also shows that the contribution of this transition has dropped compared to the titanium-complex and since the ring current has diminished in planes B and C, it could be related to this.

$[V(P_5)_2]^-$ is not discussed extensively as it serves as an intermediate from $[Ti(P_5)_2]^{2-}$ to $[Cr(P_5)_2]$ in terms of ring currents and MO-shifting. For the vanadium-complex it can also be stated that it has lost its diatropic current stretching the whole molecule. Similarly, it has a big paratropic current at the metal-centre, see appendix B3.

$[Sc(P_5)_2]^{3-}$

Figure 9 illustrates the same x-, y- and z-transitions as with titanium. Remarkably, the diamagnetic current, seen in appendix B5, on the phosphorus-ring due to the π-orbitals has vanished. The other diamagnetic currents are there albeit faintly. The transitions $E_1'' \rightarrow E_2''$ and from

HOMO to LUMO E_2' → E_2'' have become more prominent than in the titanium molecule which is also true by looking at the contributions in table 4. The x/y-translation from MOs 84 and 85 (E_1") to 98 and 99 (E_2") are more comparable in strength. Worth mentioning is that scandium and zirconium have the largest ring to ring distance with 4.029 and 3.998 Å, respectively, in table 5. Whilst titanium has a ring-ring distance of 3.654 Å that follows a decreasing trend along the periodic table until ferrocene with a distance of 3.361 Å. This could offer some insight into a loss of ring current due to a larger distance for the electrons to cross. However, the loss of ring current for the phosphorus-ring is unrelated to the distance between rings. It could be that due to the high negative charge on the complex, i.e. -3, is too much for the complex to sustain a ring current. The Rx/y-rotations have not been marked as scandium has lost the paratropic current around the centre.

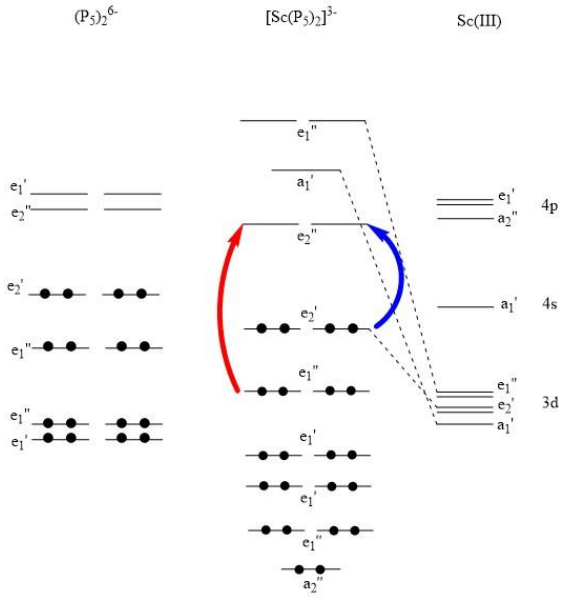

Fig. 9 *MO-diagram of $[Sc(P_5)_2]^{3-}$ with x/y- (red) and z-translations (blue).*

Table 5 *ring-to-ring distance of each metal-complex*

Complex	Distance (Å)
$[Sc(P_5)_2]^{3-}$	4.029
$[Zr(P_5)_2]^{2-}$	3.998
$[Ti(P_5)_2]^{2-}$	3.654
$[V(P_5)_2]^{-}$	3.472
$[Cr(P_5)_2]$	3.388
Ferrocene	3.361

Relative to $[Ti(P_5)_2]^{2-}$ the shifts in MOs are the swapping of LUMOs E_2'' and A_1' as well as the interchanging of occupied MOs A_2'' and E_1''. The zirconium-complex has the same relative positions of MOs as its scandium counterpart. Overall the diamagnetic ring current seems to be better intact in the zirconium-complex, as shown in appendix B6. Additionally, there is a paratropic current at the metal again in plane C.

$[Mn(P_5)_2]^+$

The manganese-complex has delivered no results for the ring currents as the geometry optimisation failed. The complex was not able to achieve a minimum energy and have the geometry optimised. The first normal mode continued to have an imaginary frequency.

Thus, what can be stated form these results is that all analysed complexes are aromatic in the ligand. Only the complexes $[Fe(C_5H_5)_2]$, $[Ti(P_5)_2]^{2-}$, $[V(P_5)_2]^{-}$, and $[Zr(P_5)_2]^{2-}$ have an uninterrupted diatropic ring current stretching the pancake bond and are thus aromatic in this direction. The complexes with vanadium and zirconium at its centre barely show this current. The zirconium, titanium, vanadium and chromium centres are anti-aromatic with vanadium and chromium having a largely increased paratropic current. Out of these results does not necessarily come forth a correlation between pancake structures and aromaticity. Further research could be done in this field to cover the origins and implications of the aromaticity some of these compounds have. Additionally, the series of pancake compounds researched in

this manner could be extended to other pancakes. This could aid in deriving a more irrefutable connection between pancakes and aromaticity. Nevertheless, the aromaticity these compounds exhibit from ring to ring does bring forth ramifications in terms of their reactivity. Aromaticity is after all a great indicator towards the likelihood of certain reactions[4].

Conclusion

Six out of seven pancake structures, i.e. $[Fe(C_5H_5)_2]$, $[Sc(P_5)_2]^{3-}$, $[Ti(P_5)_2]^{2-}$, $[V(P_5)_2]^{-}$, $[Cr(P_5)_2]$ and $[Zr(P_5)_2]^{2-}$, have a diamagnetic ring current on the rings of the ligands and, thus, are aromatic. Only the scandium-complex shows a decrease in strength of this current. The complex $[Mn(P_5)_2]^{+}$ has given no ring currents as the geometry is not able to converge to a minimum energy. Overall, the scandium-complex has lost completely all ring currents deeming it to be non-aromatic. However, the contribution of x-, y- and especially z-translations in the scandium-complex are higher than or equal to its titanium counterpart. The ring-to-ring distance is the highest for the scandium-complex with 4.029 Å whilst $[Ti(P_5)_2]^{2-}$ has a distance of 3.654 Å. This could be a cause for the diminishing of the ring current, meaning that the distance becomes too great for the delocalised electrons to bridge.

A diamagnetic ring current in the direction of the pancake bonds is visible for the complexes with iron, titanium, vanadium and zirconium at its centre. Admittedly, the ring currents for the vanadium- and zirconium-complexes are barely intact. Thus, these compounds are aromatic across the length of the molecule. $[Cr(P_5)_2]$, on the other hand, shows clearly a missing ring current in this direction. Looking at the relative positions for the MOs of $[Cr(P_5)_2]$ in comparison to the titanium-complex, a shift can be seen of the 3d-orbitals downwards. According to a group population analysis of these orbitals, electrons certainly occupy the orbitals more in the chromium-complex. Due to the increase of d-character on the orbitals some of its pancake nature could be lost which can be a causation for the loss of ring currents. The titanium-complex has an uninterrupted ring current along the pancake bonds with the highest current density out of this set of molecules.

Furthermore, an increase in paratropic ring current around the metal-centre can be seen in the vanadium- and chromium-complexes compared to the titanium-complex. The value of the contributions of the Rx/y-rotations to this current go up as well to values of 22.30 for $[Cr(P_5)_2]$. It seems that the higher charge on the metal-centre is able to draw in the electrons more to give a greater paratropic current. $[Zr(P_5)_2]^{2-}$ has a small paratropic current at the centre as well next to $[Ti(P_5)_2]^{2-}$, $[V(P_5)_2]^{-}$ and $[Cr(P_5)_2]$.

However, stating the aromaticity of some of these compounds does not inherently mean they are caused by the pancake bonds. There remains a gap of knowledge to connect the pancake bonds and aromaticity together.

References

1. Hoffmann, R. (2015). The Many Guises of Aromaticity. *American Scientist*, *103*(1), 18. https://doi.org/10.1511/2015.112.18
2. von Schleyer, P. R., & Jiao, H. (1996). What is aromaticity? *Pure and Applied Chemistry*, *68*(2), 209–218. https://doi.org/10.1351/pac199668020209
3. Wannere, C. S., & Schleyer, P. R. (2003). How Do Ring Currents Affect 1H NMR Chemical Shifts? *Organic Letters*, *5*(5), 605–608. https://doi.org/10.1021/ol027327k
4. Sundholm, D., Fliegl, H., & Berger, R. J. F. (2016). Calculations of magnetically induced current densities: theory and applications. *Wiley*

Interdisciplinary Reviews: Computational Molecular Science, *6*(6), 639–678. https://doi.org/10.1002/wcms.1270

5. Steiner, E., & Fowler, P. W. (2001a). Four- and two-electron rules for diatropic and paratropic ring currents in monocyclic π systems. *Chemical Communications*, *21*, 2220–2221. https://doi.org/10.1039/b104847n
6. Nunes dos Santos Comprido, L., Havenith, R. W. A., & Klein, J. E. M. N. On the Synergistic Noninnocent Behaviour of Two P5 Units in the Sandwich Complex [Ti(P5)2]2−, (unpublished).
7. Urnezius, E. ,W. W. Brennessel, C. J. Cramer, J. E. Ellis & P. v. R. Schleyer, (2002). A Carbon-Free Sandwich Complex [(P5)2Ti]2-. *Science*, *295*(5556), 832–834. https://doi.org/10.1126/science.1067325
8. Kertesz, M. (2018a). Pancake Bonding: An Unusual Pi-Stacking Interaction. *Chemistry - A European Journal*, *25*(2), 400–416. https://doi.org/10.1002/chem.201802385
9. Martinez, C. R., & Iverson, B. L. (2012). Rethinking the term "pi-stacking". *Chemical Science*, *3*(7), 2191–2201. https://doi.org/10.1039/c2sc20045g
10. Cui, Z.-, Lischka, H., Beneberu, H. Z., & Kertesz, M. (2014). Double Pancake Bonds: Pushing the Limits of Strong π–π Stacking Interactions. *Journal of the American Chemical Society*, *136*(37), 12958–12965. https://doi.org/10.1021/ja505624y
11. Bean, D. E., Fowler, P. W., & Morris, M. J. (2011). Aromaticity and ring currents in ferrocene and two isomeric sandwich complexes. *Journal of Organometallic Chemistry*, *696*(10), 2093–2100. https://doi.org/10.1016/j.jorganchem.2010.11.014
12. Steiner, E., Soncini, A., & Fowler, P. W. (2006). Full Spectral Decomposition of Ring Currents. *The Journal of Physical Chemistry A*, *110*(47), 12882–12886. https://doi.org/10.1021/jp063760q
13. Steiner, E., & Fowler, P. W. (2001). Patterns of Ring Currents in Conjugated Molecules: A Few-Electron Model Based on Orbital Contributions. *The Journal of Physical Chemistry A*, *105*(41), 9553–9562. https://doi.org/10.1021/jp011955m
14. Jensen, F. (2017). Introduction to Computational Chemistry (3rd ed.). Wiley.
15. Keith, T. A., & Bader, R. F. W. (1993). Calculation of magnetic response properties using a continuous set of gauge transformations. *Chemical Physics Letters*, *210*(1–3), 223–231. https://doi.org/10.1016/0009-2614(93)89127-4
16. Fitzpatrick, R. (2012). *Electromagnetism and Optics. An Introductory Course*. University of Texas.
17. Guest *, M. F., Bush, I. J., Van Dam, H. J. J., Sherwood, P., Thomas, J. M. H., Van Lenthe, J. H., Havenith, R. W. A., & Kendrick, J. (2005). The GAMESS-UK electronic structure package: algorithms, developments and applications. *Molecular Physics*, *103*(6–8), 719–747. https://doi.org/10.1080/00268970512331340592
18. Havenith, R. W. A., & Fowler, P. W. (2007). Ipsocentric ring currents in density functional theory. *Chemical Physics Letters*, *449*(4–6), 347–353. https://doi.org/10.1016/j.cplett.2007.10.083
19. P. Lazzeretti and R. Zanasi, SYSMO Package, University of Modena, Italy, 1980. Mapping routines written in Exeter.
20. Gaussian 16, Revision B.01, M. J. Frisch, G. W. Trucks, H. B. Schlegel, G. E. Scuseria, M. A. Robb, J. R. Cheeseman, G. Scalmani, V. Barone, G. A. Petersson, H. Nakatsuji, X. Li, M. Caricato, A. V. Marenich, J. Bloino, B. G. Janesko, R. Gomperts, B. Mennucci, H. P. Hratchian, J. V. Ortiz, A. F. Izmaylov, J. L. Sonnenberg, D. Williams-Young, F. Ding, F. Lipparini, F. Egidi, J. Goings, B. Peng, A. Petrone, T. Henderson, D. Ranasinghe, V. G. Zakrzewski, J. Gao, N. Rega, G. Zheng, W. Liang, M. Hada, M. Ehara,

K. Toyota, R. Fukuda, J. Hasegawa, M. Ishida, T. Nakajima, Y. Honda, O. Kitao, H. Nakai, T. Vreven, K. Throssell, J. A. Montgomery, Jr., J. E. Peralta, F. Ogliaro, M. J. Bearpark, J. J. Heyd, E. N. Brothers, K. N. Kudin, V. N. Staroverov, T. A. Keith, R. Kobayashi, J. Normand, K. Raghavachari, A. P. Rendell, J. C. Burant, S. S. Iyengar, J. Tomasi, M. Cossi, J. M. Millam, M. Klene, C. Adamo, R. Cammi, J. W. Ochterski, R. L. Martin, K. Morokuma, O. Farkas, J. B. Foresman, and D. J. Fox, Gaussian, Inc., Wallingford CT, 2016.

Appendix A

In the home screen (/home/s3429679) is a list of directories with all complexes that were researched, i.e. Ferrocene, TiP5, VP5, CrP5, MnP5, ScP5 and ZrP5. Additionally, there is a directory called ‘’P5-rings’’ which has the data for the energies and the symmetry of the $(P_5)_2^{6-}$ MOs. These are stored in the files ‘’EnergySymmetryP5rings.inp’’ and ‘’EnergySymmetryP5rings.out’’. The rest of the files in there are failed attempts to get this data. Then there is a directory ‘’Metals’’ in home which stores the data for the energy of the titanium-metal AOs which is only briefly mentioned in the report.

‘’Ferrocene.RCTest’’ is a directory with all unorganised ferrocene (D_{5h} and D_{5d}) data. All the necessary files are transferred to the directory ‘’Ferrocene”, however I haven’t deleted ‘’Ferrocene.RCTest’’ yet in case I missed a file to transfer.

The optimised geometries are stored in each respective directory as follows: /**complex**/Geo.Opt/ and then named ‘’Geo.**complex**.inp’’ and the output is plus the job-id. For the manganese-complex the optimalisation failed and there are two outputs which are the last two attempts to get a complex with non-negative frequencies. The attempts prior to these ones are deleted. Also in each Geo.Opt directory is a file for the coordinates of the molecule received from drawing it in ADF.

In /TiP5/Geo.Opt/ are two more files “EnergySymmetryTiP5.inp’’ and output plus job-id which were used to get the symmetries of the complex MOs. These were made with gaussian16 thus the order of MOs is different than with GAMESS-UK. Therefore, the shapes of the orbitals were cross-referenced to get the symmetries of the MOs with the order attained from the GAMESS-UK calculation.

The hessian calculations are stored in a similar manner as the geometry optimalisations. Thus, in /**complex**/Geo.Opt/ and then named like ‘’Hessian.**complex**.inp’’ and the output is with the job-id added.

In /**complex**/Geo.Opt/ are two more directories for TiP5 and CrP5. The first directory is called ‘’CharacterAnalysis’’ which has the data for the Mulliken electron occupation (d-character) of the 3d-orbitals on these two complexes.
The second directory “Orbitals” has the data for all povray files and respective pictures (.png) of certain MOs. For CrP5 these are the 3d-orbitals 84, 85, 88, 89 and 90 and for TiP5 these are the 3d-orbitals and more, i.e. 80, 81, 84, 85, 86, 87, 88, 89, 90, 91 and 92.

All calculations and pictures for ring currents are also in their respective complex directories: /**complex**/Ring.Current/ which are all subdivided into 4 other directories, “NormalPlane”, “SidePlane”, “CenterPlane” and “**complex**”. The place /**complex**/Ring.Current/ contains the optimised molecule placed in the XY-plane file for each complex which is used in the input for ring current calculations.

Name	Corresponding plotting plane in report
Normal plane	Plane A
Side plane	Plane B
Center plane	Plane C

The /**complex**/Ring.Current/**complex**/ directories contain the fort files generated by GAMESS-UK and the program mo801 (only for Ferrocene, TiP5, CrP5 and ScP5) which was used to

calculate the contribution of individual transitions. The input is called ‘’mo801’’ and the output is called, e.g. Fe.xyz.p.inp.job-id to indicate transition type and dia- or paratropic contribution.

In /**complex**/Ring.Current/Normalplane/ are the full inputs for a ring current analysis, thus with the optimised geometry in GAMESS-UK and then mo800 (SYSMO) for the ring current pictures. The other directories “sideplane” and ”centerplane” only have SYSMO in the input as the fort files are copied to each directory.
The ring current input is called “Normal.**complex**.inp” + output with job-id. To get the molecule in the centre of the picture, files were made called “New.Normal.**complex**.inp” plus output. The corresponding figures are then generated into postscript files (.ps) with the name “**metal**.Normal.Pi.ps” and “**metal**.Normal.Total.ps” for the systems with only π-orbitals and all orbitals, respectively.
The same system of naming files applies to the “sideplane” and “centerplane” directories with the word ‘’normal’’ exchanged with ‘’side’’ or ‘’center’’.

For CrP5 and Ferrocene 3D-models were made which were not used in the report. These files are located in /CrP5/3D/ and /Ferrocene/D5h/3D/, respectively.

Appendix C

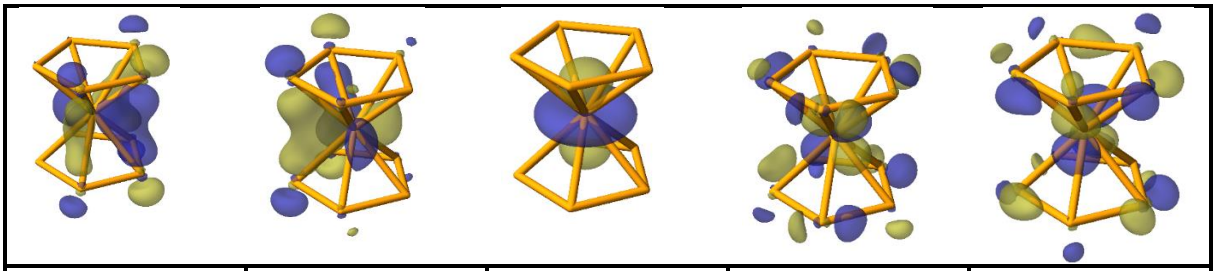

Ti-86 (x^2-y^2)	Ti-87 (xy)	Ti-88 (z^2)	Ti-91 (xz)	Ti-92 (yz)

The 3d-orbitals on the titanium centre.

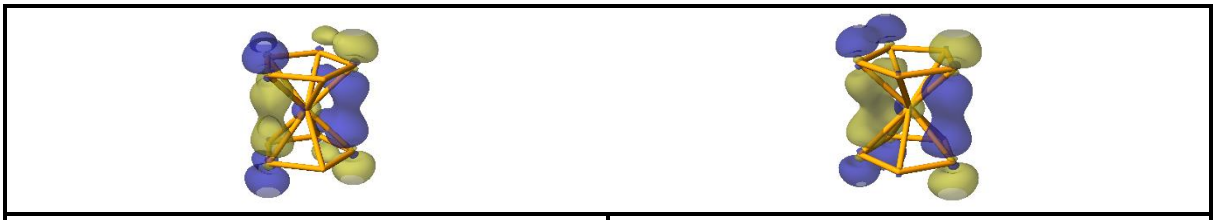

Ti-80	Ti-81

Pancake orbitals of Ti-80 and Ti-81.

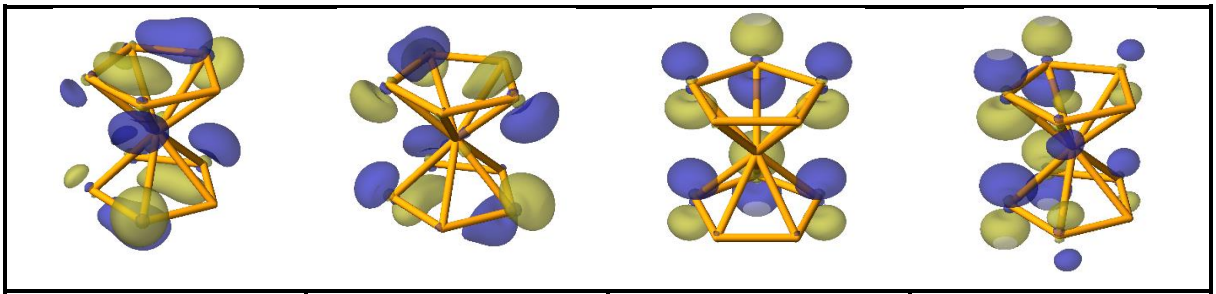

Ti-84	Ti-85	Ti-89	Ti-90

The orbitals of Ti-84, Ti-85, Ti-89 and Ti-90.

Note *These orbitals give all shapes of significant MOs in the discussed transitions. As the shapes are roughly the same with the other metal-complexes, they can be used to infer the shapes of the MOs of other complexes by looking at overlapping symmetries in figure 8.*